An examination of a partial second octant of data for **2b** showed a nearly random variation in the intensities of equivalent reflections. Hence, only a single form of the data was obtained, and this resulted in a very low data to parameter ratio. All tested samples of crystals of **3a** diffracted diffusely. The crystals appeared layered; under crossed polarizers, interference patterns were seen, indicating some offset of layers.

All computations used SHELXTL software (version 5.1) (G. Sheldrick, Nicolet XRD, Madison, WI).

Acknowledgment. We thank the Office of Basic Energy Sciences, Department of Energy, for support of this research and the National Science Foundation for providing funds to support the purchase of the X-ray diffractometer at the university of Delaware.

Supplementary Material Available: For **2b**, **3a**, **5b**, **6a'**, and **7a**, tables of anisotropic thermal parameters, bond lengths and angles, and calculated hydrogen atom positions (19 pages); tables of structure factors for the same compounds (72 pages). Ordering information is given on any current masthead page.

The Peroxide-Dependent μ_2-O Bond Formation of $[Mn^{IV}SALPN(O)]_2$

Erlund J. Larson and Vincent L. Pecoraro*

Contribution from the Department of Chemistry, Willard H. Dow Chemical Laboratories, University of Michigan, Ann Arbor, Michigan 48109-1055. *Received May 29, 1990*

Abstract: A variety of Mn^{III}SALPN complexes as monomeric and dimeric derivatives have been prepared. Acetonitrile solutions of tetragonal complexes such as $[Mn^{III}(SALPN)(CH_3OH)_2]ClO_4$, **1**, are unreactive with hydrogen peroxide unless base is added. In contrast, $[Mn^{III}(SALPN)(AcAc)]$, **2**, $[Mn^{III}(SALPN)(OCH_3)]_2$, **3**, and $Mn^{III}_2(SALPN)_3$, **4**, internally carry an equivalent of base and react rapidly to form the oxidized dimer $[Mn^{IV}(SALPN)(O)]_2$, **5**. The base is required to deprotonate hydrogen peroxide prior to reaction with **1-4**. Alkyl peroxides such as *tert*-butyl hydroperoxide also require base for reactivity but appear to follow a different mechanistic pathway consistent with the slow loss of *tert*-butoxide leading to Mn^{V}OSALPN, **19**. The conversion of **2**, **3**, or **4** to **5** has been examined with use of isotopically labeled hydrogen peroxide and ring-substituted ligand derivatives. These data demonstrate that the first intermediate in the reaction is probably a monomeric hydroperoxide adduct $[Mn^{III}(SALPN)(O_2H)]$, **16**. The monomer **16** then reacts with another equivalent of $Mn^{III}(SALPN)(X)$ to form a peroxo-bridged dimer $(SALPN)Mn^{III}(O_2)Mn^{III}(SALPN)$, **17**, which undergoes internal electron transfer forming **5**. This proposed mechanism is consistent with X-ray structural characterization of the precursors $(Mn^{III}(SALPN)(AcAc)$, **2**, $[Mn^{III}(5\text{-Cl-SALPN})(CH_3OH)_2]ClO_4$, **7**, $[Mn^{III}(3,5\text{-diCl-SALPN})(CH_3O)]_2$, **12**, and $Mn^{III}_2(SALPN)_3$, **4**) and product (**5**) complexes in the solid state and ^1H NMR spectra of the Mn(III) species in methylene-d_2 chloride/5% methanol-d_4 at 22 °C. Electrochemistry and isotope labeling experiments show that monomeric compounds such as $[Mn^{IV}(SALPN)(AcAc)]PF_6$, **6**, $Mn^{IV}O(SALPN)$, or $[Mn^{V}(O)SALPN)]ClO_4$ cannot be involved in the hydrogen peroxide-dependent transformation to form **5**. In contrast, intermediates such as **19** are implicated in the *tert*-butyl peroxide oxidations. X-ray parameters for **2**, $C_{22}H_{23}N_2O_4Mn_1$, 434 g/mol, crystal system, monoclinic ($P2_1/c$), a = 8.004 (3) Å, b = 14.035 (8) Å, c = 18.134 (6) Å, β = 83.30 (3)°, V = 2023 (2) Å^3, Z = 4, 2666 data collected with $3° < 2\theta < 45°$, 1624 data with $I > 3\sigma(I)$, R = 0.0503, R_w = 0.0503; **4**, $Mn_2N_7O_6C_{56}H_{53}$, 1029 g/mL, crystal system triclinic ($P\bar{1}$), a = 11.011 (4) Å, b = 14.103 (5) Å, c = 17.174 (7) Å, α = 74.59 (3)°, β = 83.82 (3)°, γ = 82.28 (3)°; V = 2540 (2) Å^3, Z = 2, 6104 data collected with $3° < 2\theta < 45°$, 4416 data with $I > 3\sigma(I)$, R = 0.0475, R_w = 0.0360; **7**, $C_{19}H_{22}N_2O_8MnCl_3$, 566 g/mol, crystal system, monoclinic ($P2_1/c$), a = 10.579 (4) Å, b = 17.451 (11) Å, c = 13.651 (6) Å, β = 112.75 (3)°, V = 2324 (2) Å^3, Z = 4, 2178 data collected with $3° < 2\theta < 45°$, 1693 data with $I > 3\sigma(I)$, R = 0.0524, R_w = 0.0457; **12**, $Mn_2Cl_8N_4O_7C_{37}H_{33}$, 1039 g/mL, crystal system monoclinic ($P2_1/n$), a = 9.213 (5) Å, b = 26.024 (16) Å, c = 17.992 (7) Å, β = 91.87 (4)°, V = 4312 (4) Å^3, Z = 2, 5639 data collected with $3° < 2\theta < 45°$, 3197 data with $I > 3\sigma(I)$, R = 0.0519, R_w = 0.0470.

Introduction

Manganese plays an important role in the metabolism of dioxygen and its reduced forms. Three examples are the dismutation of superoxide to hydrogen peroxide and dioxygen by the Mn superoxide dismutase,[1] the conversion of hydrogen peroxide to dioxygen and water by the Mn catalase,[2] and the four-electron oxidation of two water molecules to form dioxygen by the photosynthetic oxygen-evolving complex.[3] The latter two activities require clusters of manganese atoms, presumably since the reactions that they catalyze are multielectron processes.

In recent years, knowledge of the structural organizations of these multinuclear manganese enzymes has been placed on a more sound footing through EPR, X-ray absorption, and X-ray crystallographic studies. Both the oxygen-evolving complex[4-6] and the Mn catalase[7,8] have EPR spectral signatures indicative of coupled manganese centers. The Mn catalase has been crystallized,[9] and a low-resolution map has been presented which places

(1) (a) Ludwig, M. L.; Pattridge, K. A.; Stallings, W. C. *Metabolism and Enzyme Function*; Academic Press, Inc.: New York, 1986; p 405. (b) Stallings, W. C.; Pattridge, K. A.; Strong, R. K.; Ludwig, M. L. *J. Biol. Chem.* **1985**, *260*, 16424.

(2) (a) Penner-Hahn, J. E. In *Manganese Redox Enzymes*; Pecoraro, V. L., Ed.; Verlag-Chemie: New York, Chapter 2, in press. (b) Kono, Y.; Fridovich, I. *J. Biol. Chem.* **1983**, *258*, 13646. Beyer, W. F., Jr.; Fridovich, I. *Biochemistry* **1985**, *24*, 6460.

(3) (a) Babcock, G. T.; Barry, B. A.; Debus, R. J.; Hoganson, C. W.; Atamain, M.; McIntosh, L.; Sithole, I.; Yocum, C. F. *Biochemistry* **1989**, *28*, 9557. (b) Rutherford, A. W. *Trends Biochem. Sci.* **1989**, *14*, 227. (c) Ghanotakis, D. F.; Yocum, C. F. *Ann. Rev. Pl. Physiol.* **1990**, *41*, 255. (d) Christou, G. *Acc. Chem. Res.* **1989**, *22*, 328. (e) Pecoraro, V. L. *Photochem. Photobiol.* **1988**, *48*, 249. (f) Wieghardt, K. *Angew. Chem., Int. Ed. Engl.* **1990**, *28*, 1153. (g) Govindjee; Coleman, W. J. *Sci. Am.* **1990**, *262*, 50.

(4) Dismukes, G. C.; Siderer, Y. *Proc. Natl. Acad. Sci. U.S.A.* **1981**, *78*, 274.

(5) Hannson, O.; Aasa, R.; Vanngard, T. *Biophys. J.* **1986**, *51*, 825.

(6) (a) de Paula, J. C.; Innes, J. B.; Brudvig, G. W. *Biochemistry* **1985**, *24*, 8114. (b) de Paula, J. C.; Beck, W. F.; Brudvig, G. W. *J. Am. Chem. Soc.* **1986**, *108*, 4002.

(7) Khangulov, S. V.; Barynin, V. V.; Melik-Adamyin, V. R.; Grebenko, A. I.; Voevodskaya, N. V.; Blumenfeld, L. A.; Dobryakov, S. N.; Il'Yasova, V. B. *Bioorg. Khim.* **1986**, *12*, 741.

(8) Fronko, R.; Penner-Hahn, J. E.; Bender, C. *J. Am. Chem. Soc.* **1988**, *111*, 7554.

(9) Barynin, V. V.; Vagin, A. A.; Melik-Adamyan, V. R.; Grebenko, A. I.; Khangulov, S. V.; Popov, A. N.; Andrianova, M. E.; Vainshtein, B. K. *Sov. Phys. Dokl.* **1986**, *31*, 457.

0002-7863/91/1513-3810$02.50/0

two manganese atoms within 3.6 Å. EXAFS spectra[10-13] of the oxygen-evolving complex in a variety of oxidation states are consistent with short Mn–Mn (2.7 Å) and somewhat longer (3.3 Å) separations. It has also been suggested that at least some of these manganese ions are bridged by μ_2-O^{2-} ligands.

It is now apparent that a variety of structural motifs which exploit the Mn(III) and Mn(IV) oxidation levels can satisfy many of the structural requirements that have been extracted from the biophysical data on these enzymes. Synthetic models have been prepared which incorporate the $(\mu_2\text{-O})(Mn)_2$ and $[(\mu_2\text{-O})(Mn)]_2$ cores as dinuclear, trinuclear, and tetranuclear compounds.[3d-f] These complexes often exhibit both short Mn–Mn separations and relatively short Mn–O distances (≤1.85 Å).

One area of synthetic modelling that has not been studied extensively is the mechanism of the formation of di-μ_2-O bridged manganese complexes from their lower valent precursors. Often the preparative procedure is via the direct oxidation of an ill-defined mixture of lower valent precursor complexes by atmospheric dioxygen or peroxides. We felt that an important entry into the reactivity of manganese–oxo clusters was to understand how such materials are formed. In this regard, we have investigated the oxidation of well-defined Mn(III) mononuclear and dinuclear precursors with hydrogen peroxide and alkyl peroxides. Such studies are of interest in defining the mechanism of the Mn catalase as well as side reactions[14,15] catalyzed by the oxygen-evolving complex. These new procedures provide quantitative yields of Mn(IV) di-μ_2-O unit with the 2.7-Å separation characteristic of metal separations in the oxygen-evolving complex. A common Mn^{III}–O–O–Mn^{III} intermediate can be invoked to explain the observed formation of $[Mn^{IV}(SALPN)(O)]_2$ when hydrogen peroxide is used as the oxidant. Alkyl peroxides appear to react via a different pathway, possibly involving a Mn^{V}=O species.

Experimental Section

Materials. Salicylaldehyde [SAL], and 1,3-diaminopropane were obtained from Aldrich Chemical Co. $Mn(CH_3COO)_3\cdot 2H_2O$ and $Mn(CH_3COO)_2\cdot 2H_2O$ were obtained from Fluka Co. Both 3,5-dichlorosalicylaldehyde [3,5-Cl-SAL] and 5-chlorosalicylaldehyde [5-Cl-SAL] were obtained from Pfaltz and Bauer. Hydrogen peroxide (50% aqueous solution) was purchased from Fisher Scientific. All other chemicals and solvents were reagent grade. Tetra-*n*-butylammonium hexafluorophosphate [$TBAPF_6$] was synthesized by the metathesis of TBABr and NH_4PF_6 in water followed by three recrystallizations from absolute ethanol. For the electrochemical studies, high purity solvents (methylene chloride, dimethyl formamide [DMF], and methanol) were used as received from American Burdick and Jackson Co. High purity argon gas was used to deoxygenate solutions. All other chemicals and solvents were reagent grade. Isotopically labeled oxygen ($^{18}O_2$) and water ($H_2{}^{18}O$) were obtained from Cambridge Isotope Laboratories. Isotopically labeled hydrogen peroxide ($H_2{}^{18}O_2$) was prepared by the reduction of $^{18}O_2$ by 2-ethylanthrohydroquinone following the procedure of ref 16.

Abbreviations used: H_2SALADHP = 2-(salicylideneiminato)-2-methyl-1,3-dihydroxypropane; H_2SALAHP = 3-(salicylideneiminato)-1-hydroxypropane; H_2HIB = hydroxyisobutyric acid; H_2SALPN = 1,3-bis(salicylideneiminato)propane; H_2SALEN = 1,2-bis(salicylideneiminato)ethane; H_2SALPS = *N,N'*-[2,2'-dithiobis(phenylene)]bis(salicylideneaminato); H_2([5-Cl-SAL]PN) = 1,3-bis((5-chlorosalicylidene)-iminato)propane; H_2([3,5-diCl-SAL]PN) = 1,3-bis((3,5-dichlorosalicylidene)iminato)propane; H_2(2-OH-SALPN) = 1,3-bis(salicylideneiminato)-2-hydroxypropane; HAcAc = 2,4-pentanedione; TBA = tetra-*n*-buthylammonium cation.

Synthesis of Compounds. $[Mn^{III}(SALPN)(CH_3OH)_2]ClO_4$ **1.** (Caution! Metal perchlorate salts can be explosive.) Reaction of a suspension of 10 mmol (5.03 g) of **2** (vide infra) in 75 mL of methanol with 1.1 equiv of $HClO_4/H_2O$ (10.3 M) afforded a deep green solution. Dilution of this solution to 300 mL with diethyl ether followed by cooling to −20 °C produced green microcrystalline **1** in >90% yield. Single crystals of $[Mn^{III}(5\text{-Cl-SALPN})(CH_3OH)_2]ClO_4$, **7**, prepared similarly were used in the X-ray analysis. Element anal. Calcd for $Mn_1C_{18}H_{20}N_2O_8Cl_3\cdot H_2O$, **7**, (mw = 573): C, 37.7; H, 3.84; N, 4.88; Mn, 9.60. Found: C, 37.23; H, 3.70; N, 4.90; Mn, 9.68.

$[Mn^{III}(SALPN)(AcAc)]$, 2. Twenty mmol (3.13 g) of 5-Cl-salicylaldehyde and 10 mmol (0.833 mL) 1,3-diaminopropane were added to 150 mL of methanol under reflux resulting in a bright yellow-orange solution. After the solution was refluxed for 15 min, 10 mmol (3.52 g) of $Mn(AcAc)_3$ was added, and then the solution was cooled to −20 °C. Precipitation of green microcrystalline **2**, which was recovered by suction filtration, was achieved in >90% yield. Elemental anal. Calcd for $Mn_1C_{22}H_{23}N_2O_4$, **2** (mw = 434): C, 60.88; H, 5.30; N, 6.45; Mn, 12.67. Found: C, 60.79; H, 5.27; N, 6.45; Mn, 12.58.

$[Mn^{III}(SALPN)(OCH_3)]_2$, 3. H_2SALPN (10 mmol) and 30 mmol of sodium methoxide were reacted with 10 mmol of $Mn^{III}(acetate)_3\cdot 2H_2O$ in 250 mL of refluxing methanol by using a Schlenk line with Ar as the inert atmosphere. The resultant brown-red solution was allowed to cool in an insulated warm water bath for 24 h. Crystalline **3** was obtained in >75% yield by suction filtration in air. Single crystals of $[Mn^{III}(3,5\text{-diCl-SALPN})(OCH_2)]_2$, **12**, were used in the X-ray analysis. Elemental anal. Calcd for $Mn_2C_{36}H_{36}N_4O_6Cl_8$, **3** (mw = 1008): C, 42.89; H, 2.98; N, 5.56; Mn, 10.91. Found: C, 42.80; H, 3.01; N, 5.27; Mn, 10.53.

$[Mn^{III}_2(SALPN)_3]$ 4. H_2SALPN (15 mmol, 4.23 g) and 30 mmol of NaOH(s) (1.2 g) were added to 400 mL of methanol at 15 °C and stirred until all of the NaOH dissolved (1 h). $Mn^{III}(OAc)_3\cdot 2H_2O$ (10 mmol, 2.68 g) was then added to the solution under flush and stirred for 15 min. A green microcrystalline solid was vacuum filtered in air giving 95% yield of **4**. This was recrystallized from degassed pyridine at ~85% overall yield. Single crystals were obtained from pyridine and used for X-ray analysis. Elemental anal. Calcd for $Mn_2(SALPN)_3$, **4** (mw = 950 without pyridine): C, 64.3; H, 5.1; N, 8.8; Mn, 11.6. Found: C, 63.8; H, 5.1; N, 8.6; Mn, 11.1.

$[Mn^{IV}(SALPN)(O)]_2$, 5. Procedure (A) by reaction of **3** with dioxygen: 5 mmol (3.66 g) of **3** was dissolved in 200 mL of wet (≈1% H_2O) acetonitrile. The solution was then aerated with O_2 for 15 min. The resultant microcrystalline product, **5**, was recovered in >85% yield. Procedure (B) by reaction of **3** with hydrogen peroxide: Addition of 1.2 equiv of 50% H_2O_2 to an acetonitrile solution of **3** gives microcrystalline **5** in 96% yield. The solution was cooled to −10 °C and suction filtered. Procedure (C) by reaction of **2** with hydrogen peroxide: 10 mmol (4.34 g) of **2** was dissolved in acetonitrile with no effort to exclude water or O_2. Hydrogen peroxide (50% aqueous, 1.2 equiv) was added, and an instantaneous color change to blood-red was noted along with formation of plate-like crystals. The solution was immediately cooled to −10 °C and suction filtered giving 100% yield of **5**. Procedure (D) by reaction of **3** with *tert*-butylOOH: 10 mmol (4.34 g) of **2** was dissolved in 150 mL of wet acetonitrile under argon. To this was added 5 mmol of *tert*-butylOOH, and the blood-red mixture was stirred for 1.5 h at room temperature. Plates of **5** were isolated in 80% yield upon suction filtration in air. The X-ray structure of this molecule has been reported previously.[17] Elemental anal. Calcd for $Mn_2C_{34}H_{32}N_4O_4\cdot$DMF, **5** (mw = 775): C, 57.3; H, 5.03; N, 9.03; Mn, 14.2. Found: C, 57.6; H, 5.3; N, 9.4; Mn, 14.0. FAB mass spectral parent ion peak at 702.

$[Mn^{IV}(3,5\text{-diCl-SALPN})(AcAc)]PF_6$, 6. Controlled potential bulk electrolysis of **10** at +800 mV vs SCE in methylene chloride with 0.15 M $TBAPF_6$ as supporting electrolyte gave **6**. Coulometry indicated a 98% yield based on 1 electron/Mn. The solution was diluted to twice the original volume with use of toluene and cooled to −20 °C. After removal of crystalline electrolyte by suction filtration, a second crop of needles, **6** was isolated by filtration. Elemental anal. Calcd for $Mn_1C_{22}H_{19}N_2O_4Cl_4PF_6$, **6** (mw = 717): C, 36.85; H, 2.65; N, 3.91; Mn, 7.67. Found: C, 37.64; N, 2.63; N, 3.86; Mn, 7.37.

$[Mn^{III}(SALPN)(CF_3SO_3)OH_2]\cdot CH_3OH$, 13. Reaction of a suspension of 10 mmol (5.03 g) of **2** in 75 mL of acetonitrile with 1.1 equiv of triflic

(10) (a) Yachandra, V. K.; Guiles, R. D.; McDermott, A.; Britt, R. D.; Dexheimer, S. L.; Sauer, K.; Klein, M. P. *Biochim. Biophys. Acta* **1986**, *850*, 324. (b) Yachandra, V. K.; Guiles, R. D.; McDermott, A.; Cole, J. L.; Britt, R. D.; Dexheimer, S. L.; Sauer, K.; Klein, M. P. *Biochemistry* **1987**, *26*, 5974. (c) Kirby, J. A.; Goodin, D. B.; Wydrzynski, T.; Robertson, A. S.; Klein, M. P. *J. Am. Chem. Soc.* **1981**, *103*, 5529. (d) Kirby, J. A.; Robertson, A. S.; Smith, J. P.; Thompson, A. C.; Cooper, S. R.; Klein, M. P. *J. Am. Chem. Soc.* **1981**, *103*, 5537.

(11) (a) Guiles, R. D.; McDermott, A.; Yachandra, V. K.; Cole, J. L.; Dexheimer, S. L.; Britt, R. D.; Wieghardt, K.; Bossek, U.; Sauer, K.; Klein, M. P. *Biochemistry* **1990**, *29*, 471. (b) Guiles, R. D.; Yachandra, V. K.; McDermott, A.; Cole, J. L.; Dexheimer, S. L.; Britt, R. D.; Sauer, K.; Klein, M. P. *Biochemistry* **1990**, *29*, 486.

(12) George, G. N.; Prince, R. C.; Cramer, S. P. *Science* **1989**, *243*, 789.

(13) Penner-Hahn, J. E.; Fronko, R.; Pecoraro, V. L.; Bowlby, N. F.; Betts, S. D.; Yocum, C. F. *J. Am. Chem. Soc.* **1990**, *112*, 2549.

(14) Velthuys, B.; Kok, B. *Biochim. Biophys. Acta* **1978**, *502*, 211.

(15) Frasch, W.; Mei, R. *Biochemistry* **1987**, *26*, 7321. Mano, J.; Takahashi, M.; Asaka, K. *Biochemistry* **1987**, *26*, 2495.

(16) Sitter, A. J.; Terner, J. *J. Label. Compds. Radiopharm.* **1984**, *22*, 461.

(17) Larson, E.; Lah, M. S.; Li, X.; Bonadies, J. A.; Pecoraro, V. L. Submitted to *Inorg. Chem.*

Table I. Crystallographic Parameters for **7**, **2**, **12**, and **4**

	7	2	12	4
formula	$Mn_1O_8Cl_3N_2C_{19}H_{22}$	$Mn_1O_4N_2C_{22}H_{23}$	$Mn_2Cl_8N_4O_7C_{37}H_{33}$	$Mn_2O_6N_7C_{56}H_{53}$
mol wt	566	434	1039	1029
a, Å	10.579 (4)	8.004 (3)	9.213 (5)	11.011 (4)
b, Å	17.451 (11)	14.035 (8)	26.024 (16)	14.103 (5)
c, Å	13.651 (6)	18.134 (6)	17.992 (7)	17.174 (7)
				74.59 (3)
β, deg	112.75 (3)	83.30 (3)	91.87 (4)	83.82 (3)
				82.28 (3)
V, Å^3	2324 (2)	2023 (2)	4312 (4)	2540 (2)
cryst syst	monoclinic	monoclinic	monoclinic	triclinic
space group	$P2_1/c$	$P2_1/c$	$P2_1/n$	$P\bar{1}$
d_{calc}, g/mL	1.62	1.42	1.61	1.35
d_{obs}, g/mL	1.63	1.40	1.59	1.38
Z	4	4	2	2
radiation	Mo Kα (0.7107 Å)	Mo Kα (0.7107 Å)	Mo Kα (0.7107 Å)	Mo Kα (0.7107 Å)
abs coeff, μ (cm^{-1})	15.0	6.16	11.1	5.4
cryst size (mm)	0.22 × 0.18 × 0.16	0.19 × 0.15 × 0.07	0.04 × 0.34 × 0.52	0.5 × 0.1 × 0.3
scan speed (deg/min)	2.5–12	2.5–12	2.5–12	2.5–12
scan range (deg)	$3 < 2\theta < 45$	$3 < 2\theta < 45$	$3 < 2\theta < 45$	$5 < 2\theta < 45$
unique data collected	2178	2666	5639	6104
obsd data ($I > 3\sigma(I)$)	1693	1624	3197	4416
largest nonsolv res	0.55	0.34	0.57	0.42
R	0.0524	0.0503	0.0519	0.0475
R_w	0.0457	0.0503	0.0471	0.0360

acid afforded a deep brown solution. Dilution of this solution to 300 mL with diethyl ether followed by cooling to −20 °C produced brown microcrystalline **13** in >98% yield. Elemental anal. Calcd for $Mn_1C_{19}N_2O_7N_2F_3S_1H_{22}$, **13**, (mw = 484): C, 42.7; H, 4.2; N, 5.2; Mn, 10.3. Found: C, 42.4; H, 4.2; N, 5.6; Mn, 10.45. Other complexes used in this study follow the numerical designations: $[Mn^{III}(5\text{-Cl-SALPN})(CH_3OH)_2]ClO_4$, **7**, $[Mn^{III}(3,5\text{-diCl-SALPN})(CH_3OH)_2]ClO_4$, **8**, $[Mn^{III}(5\text{-Cl-SALPN})(AcAc)]$, **9**, $Mn^{III}(3,5\text{-diCl-SALPN})(AcAc)]$, **10**, $[Mn^{III}(5\text{-Cl-SALPN})(OCH_3)]_2$, **11**, and $[Mn^{III}(3,5\text{-diCl-SALPN})(OCH_3)]_2$, **12**.

Methods

^{1}H NMR Spectroscopy. ^{1}H NMR spectra of the model complexes were obtained on a Bruker 360 MHz FT-NMR spectrometer operating in the quadrature detection mode (^{1}H frequency, 360.1 MHz). Spectra were collected by using a one-pulse sequence with a 90° pulse of 9.9 μs. Between 3000 and 10 000 transients were accumulated over a 50-kHz bandwidth for each sample. The spectra contained 8K data points, and the signal-to-noise ratio was improved by apodization of the free induction decay, which introduced a negligible 10–20 Hz line broadening. Chemical shifts were referenced to TMS or resonances due to residual protons present in the deuterated solvents.

Mass Spectrometry. Negative ion, fast atom bombardment (FAB) mass spectra were recorded on a VG 70-250-S mass spectrometer (VG Instruments, Manchester, UK). It was equipped with the standard VG FAB ion source and an Ion Tech Saddle-field atom gun. Xenon was used for the bombarding atom beam, with the atom gun controller set to 1 A and 8 kV. The samples were dissolved in 3-nitirobenzyl alcohol, obtained from Aldrich Chemical Co. The mass spectrometer was used in the negative ion detection mode, with the accelerating voltage set to 8 kV.

Electrochemistry. Cyclic voltammetry and bulk electrolysis studies were completed on a Bioanalytical Systems BAS-100 Electrochemical Analyzer. Cyclic voltammograms were generated by using platinum bead, platinum wire, and saturated calomel [SCE, within a Luggin probe] electrodes as the working, auxiliary, and reference electrodes, respectively, in a three-electrode configuration. Bulk electrolyses utilized either a platinum basket or platinum screen for working and auxiliary electrodes, each being separated by a fine frit. Tetrabutylammonium hexafluorophosphate [$TBAPF_6$] was used as the supporting electrolyte at 0.1 M concentration. All potentials were reported against the ferrocene/ferrocenium couple employed as an external reference.

X-ray Crystallography. Single crystals of **7**, **2**, and **12** were grown from methanol solutions, and **4** was crystallized from pyridine. Each crystal was then mounted in a glass capillary, and data were collected on a Syntex $P2_1$ diffractometer. Intensity data were obtained by using Mo Kα radiation (0.7107 Å) monochromatized from a graphite crystal whose diffraction vector was parallel to the diffraction vector of the sample. Three standard reflections were measured every 97 reflections. Lattice parameters were determined from a least-squares refinement of 15 reflection settings obtained from an automatic centering routine. Table I contains a summary of data collection conditions and results for each structure. The data were reduced by using the SHELX76 program package, and the structure was solved by using SHELXTL PLUS for **7**, **12**, and **4**. The SHELX86[18] Patterson solution routine was used to solve **2**. In the subsequent refinement, the function $\sum w(|F_o| - |F_c|)^2$ was minimized where $|F_o|$ and $|F_c|$ are the observed and calculated structure factor amplitudes. The agreement indices $R_1 = \sum||F_o| - |F_c||/|F_o|$ and $R_2 = [\sum w(|F_o| - |F_c|)^2/\sum w|F_o|^2]^{1/2}$ were used to evaluate the results. Atomic scattering factors are from *The International Tables for X-ray Crys-*

Table II. Selected Distances (Å) and Angles (deg) for $[Mn^{III}(SALPN)(AcAc)]$, **2**, $[Mn^{III}(SALPN)(CH_3OH)_2]ClO_4$, **7**, and $Mn^{III}_2(SALPN)_3$, **4**

2

Mn–O1	1.888 (5)	Mn–O3	1.984 (6)	Mn–N1	2.197 (6)
Mn–O2	1.884 (5)	Mn–O4	2.202 (5)	Mn–N2	2.006 (6)

O1–Mn–O2	89.7 (3)	O2–Mn–N2	89.9 (3)
O1–Mn–O3	91.6 (3)	O3–Mn–O4	84.0 (2)
O1–Mn–O4	93.3 (2)	O3–Mn–N1	83.3 (2)
O1–Mn–N1	87.1 (2)	O3–Mn–N2	90.4 (3)
O1–Mn–N2	172.6 (2)	O4–Mn–N1	167.3 (3)
O2–Mn–O3	174.4 (2)	O4–Mn–N2	94.0 (2)
O2–Mn–O4	90.5 (2)	N1–Mn–N2	86.1 (2)
O2–Mn–N1	102.2 (3)		

7

Mn1–O1	1.862 (6)	Mn1–O3	2.250 (5)	Mn1–N1	2.031 (8)
Mn1–O2	1.896 (6)	Mn1–O4	2.272 (6)	Mn1–N2	2.034 (8)

O1–Mn1–O2	83.8 (3)	O2–Mn1–N1	90.4 (3)
O1–Mn1–O3	87.9 (2)	O2–Mn1–N2	175.2 (3)
O1–Mn1–N1	174.0 (3)	O3–Mn1–N1	93.6 (2)
O1–Mn1–N2	91.6 (3)	O3–Mn1–N2	88.1 (2)
O2–Mn1–O3	90.4 (2)	N1–Mn1–N2	94.2 (3)

4

Mn1–O1	1.916 (5)	Mn1–N3	2.056 (7)	Mn2–O6	1.887 (4)
Mn1–O3	1.896 (5)	Mn1–N4	2.233 (6)	Mn2–N2	2.337 (6)
Mn1–O4	1.901 (6)	Mn2–O2	1.911 (5)	Mn2–N5	2.280 (6)
Mn1–N1	2.267 (5)	Mn2–O5	1.917 (6)	Mn2–N6	2.045 (8)

O1–Mn1–O3	178.4 (3)	O2–Mn2–O5	92.7 (2)
O1–Mn1–O4	92.1 (2)	O2–Mn2–N2	84.7 (2)
O1–Mn1–N1	86.7 (2)	O2–Mn2–N5	86.2 (2)
O1–Mn1–N3	91.1 (3)	O2–Mn2–N6	90.4 (3)
O1–Mn1–N4	87.3 (2)		

(18) Computations were carried out on an Amdahl 5860 computer. Computer programs used during the structural analysis were from the SHELX program package by George Sheldrick, Institute für Anorganische Chemie der Universitat, Gottingen, Federal Republic of Germany. Other programs used included ORTEP, a thermal ellipsoid drawing program by C. K. Johnson, and the direct methods programs MULTRAN78 by Peter Main.

Table III. Selected Distances (Å) and Angles (deg) for $[Mn^{III}(SALPN)(CH_3O)]_2$, **12**, and $[Mn^{IV}(SALPN)(O)]_2$, **5**

12

Mn1–O1	1.924 (5)	Mn2–O4	1.921 (5)	Mn1–N2	2.078 (6)
Mn1–O2	1.890 (5)	Mn2–O5	1.901 (5)	Mn2–N3	2.264 (6)
Mn1–O3	1.899 (5)	Mn2–O6	1.910 (5)	Mn2–N4	2.071 (6)
Mn1–O6	2.209 (5)	Mn1–N1	2.277 (6)	Mn1–Mn2	3.192 (3)
Mn2–O3	2.220 (5)				

Mn1–O3–Mn2	101.1 (3)	O3–Mn1–O6	78.5 (3)
Mn1–O6–Mn2	101.4 (2)	O6–Mn2–O3	78.2 (3)
O1–Mn1–O2	87.1 (2)	O3–Mn1–N1	89.5 (3)
O4–Mn2–O5	87.9 (2)	O6–Mn2–N3	93.3 (3)
O1–Mn1–O3	95.8 (2)	O3–Mn1–N2	91.7 (3)
O4–Mn2–O6	97.4 (2)	O6–Mn2–N4	90.5 (3)
O1–Mn1–O6	97.4 (2)	O6–Mn1–N1	168.0 (3)
O4–Mn2–O3	99.8 (2)	O3–Mn2–N3	171.2 (3)
O1–Mn1–N1	84.7 (3)	O6–Mn1–N2	94.9 (3)
O4–Mn2–N3	85.1 (2)	O3–Mn2–N4	94.5 (3)
O1–Mn1–N2	166.7 (2)	N1–Mn1–N2	84.3 (3)
O2–Mn1–N2	87.3 (3)	N3–Mn2–N4	83.0 (3)
O5–Mn2–N4	87.1 (3)		

5

Mn1–O1	1.928 (5)	Mn1–N1	2.006 (6)	Mn1–O3′	1.817 (5)
Mn1–O2	1.907 (5)	Mn1–N2	2.067 (6)	Mn1–Mn1′	2.731 (2)
Mn1–O3	1.808 (5)				

Mn1–O3–Mn1	97.8 (3)	O3–Mn1–N2	171.8 (2)
O1–Mn1–O2	87.2 (2)	N1–Mn1–N2	84.4 (2)
O1–Mn1–O3	92.4 (2)	O4–Mn2–N4	164.9 (3)
O1–Mn1–N1	86.3 (2)	O2–Mn1–O3	170.7 (3)
O1–Mn1–N2	95.3 (2)	O2–Mn1–O6	92.3 (3)
O2–Mn1–O3	95.4 (2)	O5–Mn2–O6	167.5 (3)
O2–Mn1–N1	169.3 (2)	O5–Mn2–O3	89.7 (3)
O2–Mn1–N2	87.7 (2)	O2–Mn1–N1	99.6 (3)
O3–Mn1–N1	93.4 (2)	O5–Mn2–N3	98.6 (3)

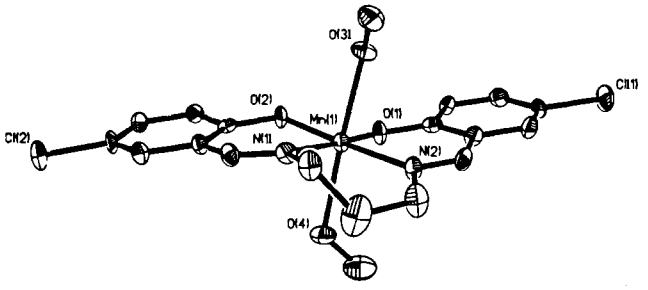

Figure 1. ORTEP plot of $[Mn^{III}(5\text{-Cl-SALPN})(CH_3OH)_2]ClO_4$, **7**, showing numbering schemes for manganese and heteroatoms only with 30% probability ellipsoids.

tallography.[19] Hydrogen atoms were located, but not refined, and placed at fixed distances from bonded carbon atoms of 0.86 Å in the final least-squares refinement. All hydrogen atoms were given fixed U values (isotropic temperature factors) of 0.08 Å.^{2} Fractional atomic coordinates for all non-hydrogen atoms of **7**, **2**, **12**, and **4** are deposited as supplementary material. Unique data and final R indices are reported in Table I. Tables II and III list selected bond distances and angles for the complexes.

Additional Methods. UV–visible spectra were recorded on a Perkin-Elmer Lambda 9 UV–vis/near-IR spectrophotometer equipped with a Perkin-Elmer 3600 data station. Infrared spectra were obtained on a Nicolet 60-SX FT-IR as KBr pellets. Solid-state magnetic susceptibilities were determined by using a Johnson-Matthey magnetic susceptibility balance [MSB-1] and by using $Hg[Co(SCN)_4]$ as a calibration standard. Solution magnetic susceptibilities were determined by using the Evans method[20] with a 360-MHz Bruker FT-NMR spectrometer. Magnetic moments from both methods are reported on a per manganese basis unless otherwise specified. Chemical analyses were performed by either Galbraith Laboratories, Inc., Knoxville, TN or the Chemical Analysis Laboratory, University of Michigan, Ann Arbor, MI.

(19) *International Tables for X-ray Crystallography*; Ibers, J., Hamilton, W., Eds.; Kyoch: Birmingham, England, 1974; Vol. IV, Tables 2.2 and 2.3.1.
(20) Bartle, K. D.; Dale, B. J.; Jones, D. W.; Maricic, J. *J. Magn. Reson.* **1973**, *12*, 286. Evans, D. F. *J. Chem. Soc.* **1959**, 2003.

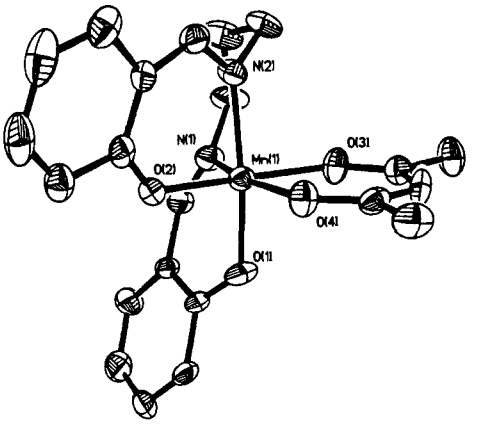

Figure 2. ORTEP plot of $[Mn^{III}(SALPN)(AcAc)]$, **2**, showing numbering schemes for manganese and heteroatoms only with 30% probability ellipsoids.

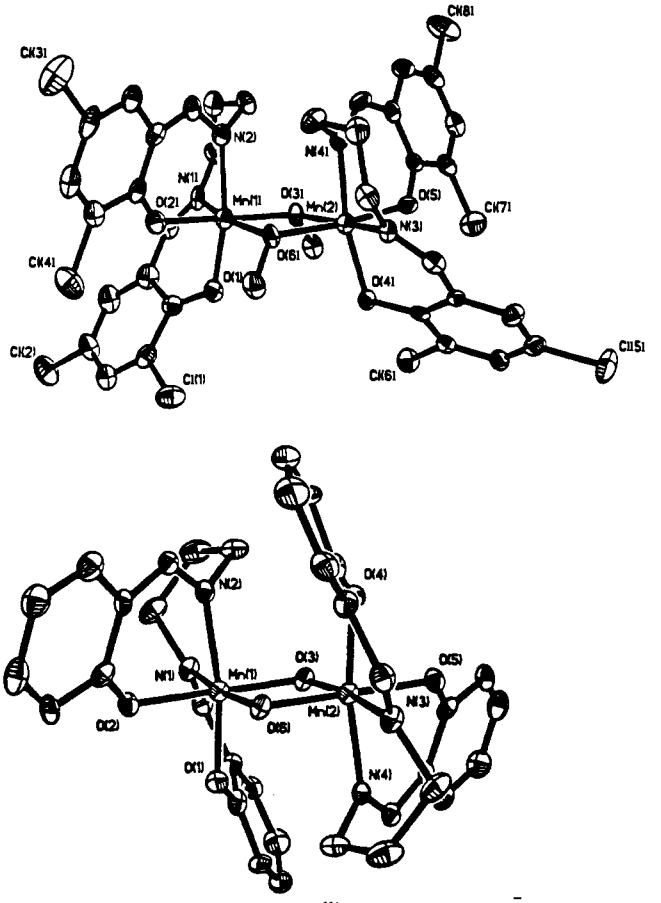

Figure 3. ORTEP plot of (top) $[Mn^{III}(3,5\text{-diCl-SALPN})(OCH_3)]_2$, **12**, and (bottom) $[Mn^{IV}SALPN(O)]_2$, **5**, from ref 17 showing numbering schemes for manganese and heteroatoms only with 30% probability ellipsoids.

Results and Discussion

Structural description of $[Mn^{III}(5\text{-Cl-SALPN})(CH_3OH)_2](ClO_4)$, 7, $Mn^{III}(SALPN)(AcAc)$, 2, $[Mn^{III}(3,5\text{-diCl-SALPN})(CH_3O)]_2$, 12, and $Mn^{III}_2(SALPN)_3$, 4. ORTEP diagrams of **7**, **2**, **12**, and **4** are provided as Figures 1–4. Table II provides a list of important bond lengths and angles for **2** and **7**, while Table III presents this information for **4**, **5**, and **12**. Previous descriptions of mononuclear Mn(III) complexes with ligands such as SALEN, SALPN, and their derivatives have all formed the tetragonally distorted trans isomer with phenolate oxygen and imine nitrogens forming a plane.[21–24] The Jahn–Teller distortion for these

(21) Pecoraro, V. L.; Butler, W. M. *Acta Crystallogr.* **1986**, *C42*, 1151.

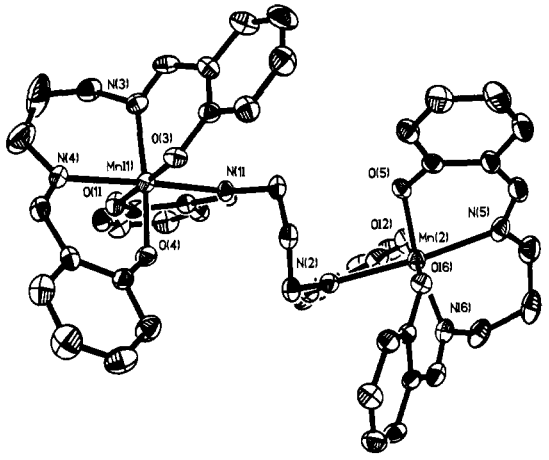

Figure 4. ORTEP plot of $Mn^{III}_2(SALPN)_3$, **4**, showing numbering schemes for manganese and heteroatoms only with 30% probability ellipsoids.

high-spin d^4 compounds is expected along the axis containing the monodentate anion or solvent molecules. This geometry is also observed for **7** with in-plane distances significantly shorter than for the axially coordinated methanols.

Because acetonylacetate is a bidentate ligand, **2** deviates from this trend. While the SALPN ligand remains tetradentate, the cis-β isomer results to accommodate the bidentate AcAc ligand. Thus **2**, unlike previous tetragonal mononuclear Mn(III) complexes, is pretemplated into the configuration required for the $[Mn^{IV}(SALPN)(O)]_2$, **5**. It is reasonable to expect that in this pretemplated configuration the imine nitrogens may be stronger donors than in the planar form. A similar effect has been seen by Collins et al.[35] by using amide donors and may contribute (vide infra) in this manganese system to the >600 mV stabilization of the Mn(IV) oxidation level in **2** as compared to the tetragonal **1**. The Jahn–Teller distortion in **2** is observed along the O4–Mn–N1 axis (Mn–O4 = 2.201 Å vs Mn–O3 = 1.986 Å; Mn–N1 = 2.203 Å vs Mn–N2 = 2.008 Å). The remaining bond distances and angles reported in Table III are unexceptional and parallel those for Mn^{III}(SALEN) derivatives.[21-24]

Numerous dimeric types have previously been reported for tetra- and pentadentate manganese Schiff base complexes. The di-μ-oxo linkage has been verified[17] for $[Mn^{IV}(SALPN)O]_2$, **5**, as shown in Figure 3. The SALPN ligand adopts the cis-β geometry. Alternatively, the trans configuration can be maintained by using a di-μ-phenolato bridge as observed in the solid state for the weakly associated Mn(SALEN)Cl[21] or the Mn(II) dimer [Mn(SALPS)]$_2$.[25] In general, SALEN derivatives form trans isomers, while SALPN (having additional flexibility imparted by the extra methylene unit) can form trans- or cis-β conformers depending on the bridging ligands. Monoalkoxy- and dialkoxy-bridged dimers of Mn^{III}(2-OH-SALPN) have also appeared.[26-27] In the latter structures the 2-OH-SALPN acts as a dinucleating ligand.

The dinuclear complex $[Mn^{III}_2(SALPN)_3]$, **4**, contains two SALPN ligands in the cis-β geometry with a third acting as a binucleating agent which occupies the two remaining cis positions on each metal center. The two manganese ions are thus tethered by the three-carbon backbone of SALPN making them essentially magnetically isolated. Each Mn(III) ion has a first coordination sphere identical in charge and ligand geometry with **2** and having similar donor capacity. The Jahn–Teller axis on each Mn(III) ion is observed along the axis containing trans imine nitrogens (N1–Mn1–N4 and N2–Mn2–N5). Selected bond distances and angles are reported in Table III. The $[Mn^{III}$(3,5-diCl-SALPN)$(CH_3O)]_2$, **12**, provides the first example of a dialkoxide-bridged Mn(III) dimer having Jahn–Teller distortions along two of the Mn–OR bonds. Once again the SALPN ligand adopts the cis-β configuration seen for **5**; however, the symmetric $(Mn^{IV}O)_2$ plane gives way to a highly distorted $[Mn^{III}(OR)]_2$ core. The $[Mn^{IV}(O)]_2$ dimer has inversion symmetry, while the $[Mn^{III}(OR)]_2$ contains a pseudo C_2 axis. Both methyl groups of the bridging methoxides are canted downward away from the propyl backbone of the ligand, presumably to minimize steric repulsion. The Mn–Mn separation in **5** is 2.72 Å while in **12** it is 3.19 Å, and the two Mn(IV)–oxo distances are 1.81 Å while the Mn(III)–O3 and Mn(III)–O6 distances are 1.90 and 2.21 Å, respectively. The 0.31-Å difference in Mn–alkoxide distances is a direct result of the Jahn–Teller distortion along the N1–Mn–O3′ axis. This weakening of the Mn(III)–O3′ bond and the substitution liability of Mn(III) explains why this dimeric complex can easily dissociate into monomeric units in solution (vide infra). Additional bond distances and angles for **12** are provided in Table III.

Table IV. Spectroscopic Properties of **1**, **2**, **4**, and **1** + NEt_3

	trans geometry		cis-β geometry	
	1	**1** + NEt_3	**2**	**4**
phenolate ring protons (ppm)	−24.5	−27.6	−23.0	−22.8
	−21.1	−25.7	−14.1	−21.0
			−8.8	−18.7
			−6.1	−16.9
			−1.1	−12.1
			+9.8	−4.8
			+58.3	−2.6
alkane backbone protons (ppm)	+20.0	+18.0	+18.1	+20.0
				+22.3
other			+38.0 (AcAc)	

^{1}H NMR of Complexes. In previous reports,[24,28] we have shown that monitoring the isotropically shifted proton resonances of Mn(III) phenolates provides useful information for understanding dimerization processes, solution speciation, and reactivity of manganese complexes. ^{1}H NMR shifts for the complexes described herein are provided in Table IV. Figure 5 shows the paramagnetic NMR spectra of complexes **1**–**4** under different conditions in methylene-d_2 chloride. The spectra are referenced to $(CH_3)_4Si$ with downfield shifts taken as positive. These features are the result of the mechanism of spin delocalization which gives rise to large chemical shifts for the phenolate protons.[29] Complexes **1** and **15** are unreactive with H_2O_2, while **2**, **3**, and **4** react rapidly with this oxidant to generate **5**. Discovery of the basis for this differential reactivity in Mn(III) precursors lends insight into the likely reaction pathway. Some pertinent questions include the following: Can initiation of the reaction with H_2O_2 be achieved without the precursor assuming the cis-β ligand configuration seen in **2**–**4**? If so, is the presence of a good proton acceptor the feature necessary for reactivity? To address these questions we examined the ^{1}H NMR spectra of **1**–**4** and their chlorine-substituted analogues.

The ^{1}H NMR spectra obtained for **1** is shown in Figure 5A, and the corresponding numerical data are contained in Table IV. The spectrum contains three proton resonances that lie outside the diamagnetic region (ca. 0–10 ppm). Two relatively sharp peaks are observed upfield and one broad peak downfield. It is possible to assign the upfield proton resonances to the 4′ (−25.0 ppm) and 5′ (−22.6 ppm) ring protons by using ring-substituted derivatives. The downfield resonance (+19.0 ppm) may arise from the protons on the 2-C atom of the propane backbone based on the examination of the ^{1}H NMR of structurally related complexes such as Mn(SALEN)X[24] (which features an ethane backbone and does

(22) Srinivasan, K.; Michaud, P.; Kochi, J. K. *J. Am. Chem. Soc.* **1986**, *108*, 2309.
(23) Gohdes, J. W.; Armstrong, W. H. *Inorg. Chem.* **1988**, *27*, 1841.
(24) Li, X.; Pecoraro, V. L. *Inorg. Chem.* **1989**, *28*, 3403.
(25) Kessissoglou, D. P.; Butler, W. M.; Pecoraro, V. L. *Inorg. Chem.* **1986**, *25*, 495.
(26) Bonadies, J. A.; Lah, M. S.; Kirk, M. L.; Kessissoglou, D. P.; Hatfield, W.; Pecoraro, V. L. *Inorg. Chem.* **1989**, *27*, 2037.
(27) Nishida, Y.; Oshino, N.; Tokii, T. *Z. Naturforsch.* **1988**, *43B*, 472.
(28) Bonadies, J. A.; Maroney, M. L.; Pecoraro, V. L. *Inorg. Chem.* **1989**, *27*, 2044.
(29) Pyrz, J. W.; Roe, A. L.; Stern, L. J.; Que, L., Jr. *J. Am. Chem. Soc.* **1985**, *107*, 614.

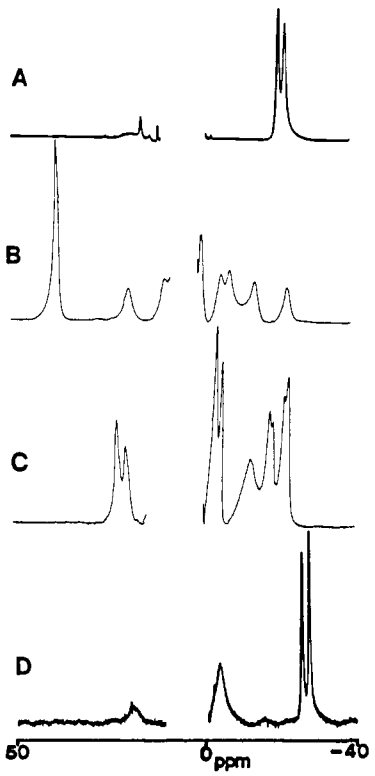

Figure 5. Hyperfine-shifted ^{1}H-NMR spectra of (A) $[Mn^{III}(SALPN)(CH_3OH)_2]ClO_4$, **1**, (B) $[Mn^{III}(SALPN)(AcAc)]$, **2**, (C) $Mn^{III}_2(SALPN)_3$, **4**, and (D) **1** plus 1 equiv of triethylamine. All spectra were taken in methylene chloride-d_2/5% methanol-d_4 at 22 °C.

not show a downfield shifted peak) and [Mn(2-OH-SALPN)$(CH_3OH)_2$], which has a substituted propane[28] backbone (+28.6 ppm) whose resonance disappears upon formation of an alkoxy-bridged dimer, $[Mn(2\text{-}OH\text{-}SALPN)]_2(CH_3OH)$.[26]

A much more complex pattern is observed for **2**–**4**. Five broad upfield resonances and three low field resonances are seen in the spectrum of **2** (Figure 5, B). The six methyl protons of coordinated AcAc are shifted far downfield (+38.2 ppm). The seven other resonances result from phenolate protons not yet unambiguously assigned. A different extent of charge transfer is expected for phenolate hydrogens that are trans to an imine nitrogen atom versus those trans to a carbonyl oxygen atom of AcAc and should cause the observed magnetic inequivalence. Two of the upfield resonances disappear in the spectra of Mn^{III}(5-Cl-SALPN)(AcAc) and Mn^{III}(3,5-diCl-SALPN)(AcAc). This suggests that two of these resonances arise from the 4-H, while two are associated with the 5-H position. The SALPN ligand is constrained in the cis-β configuration, so the two backbone methylene protons also become magnetically inequivalent. Spectra of similar complexity are obtained for **3** (not shown) and **4** (Figure 5C). The spectra obtained from complexes containing the cis-β ligand geometry (**2**, **3**, and **4**) are thus very different from those having the trans geometry (**1** and **13**). NMR spectroscopy proves to be a useful probe of the ligand conformation (trans- or cis-β) for these Mn^{III}SALPN complexes in solution.

Compound **1** (or **13**) is unreactive with H_2O_2 when dissolved in methanol, DMF, or acetonitrile; however, addition of a base such as NaOH or NaOMe leads to rapid formation of $[Mn^{IV}O(SALPN)]_2$. ^{1}H NMR has demonstrated that **1** converts to **3** if NaOMe is added to a degassed acetonitrile solution. This might suggest that H_2O_2 would react only with the pretemplated cis-β configuration (**3**) but not with the trans conformer (**1**) to generate **5** (cis-β configuration). This hypothesis was disproven by adding a stoichiometric amount of triethylamine to an acetonitrile solution of **1**. The NMR spectrum (Figure 5D) retains the resonances for the trans form, while the reaction with H_2O_2 proceeds yielding **5**. We conclude that it is more likely the base, not the ligand conformation, that is essential for initiation of this reactivity.

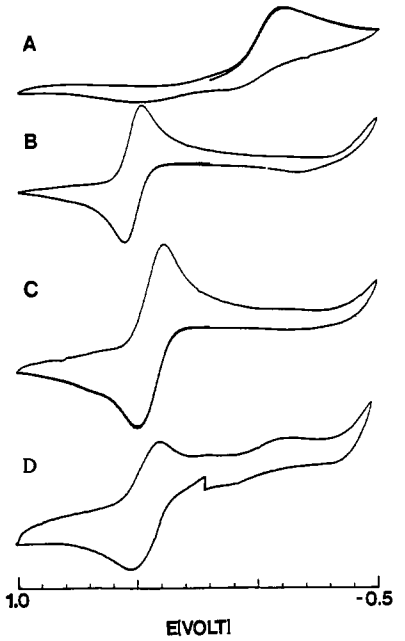

Figure 6. Cyclic voltammograms of (A) $[Mn^{III}(SALPN)(CH_3OH)_2]ClO_4$, **1**, (B) $[Mn^{III}(SALPN)(AcAc)]$, **2**, (C) $Mn^{III}_2(SALPN)_3$, **4**, and (D) $[Mn^{III}(SALPN)(OCH_3)]_2$, **3**, containing a small amount of **1**. All electroactive species are at approximately 4 mM. Potentials are referenced to SCE with use of the ferrocene/ferrocinium couple as an external standard. Supporting electrolyte is 0.1 M tetrabutylammonium hexafluorophosphate. Scan rates = 220 mV/s.

Table V. Electrochemical Behavior of Complexes

	E_{Pc} (mV)	i_c (μA)	E_{Pa} (mV)	i_a (μA)	i_c/i_a	$E_{Pc} - E_{Pa}$ (mV)
1	−106	6.3				
2	+482	27	+554	27.6	0.98	72
4	+391	17.0	+490	17.0	1.0	99
3	+383	4.2	+519	4.0	1.05	136

Additional reactivity studies are consistent with this assertion. Reaction of **1** or **13** with sodium peroxide in anhydrous DMF allows for quantitative production of **5**, implicating deprotonated hydrogen peroxide as the reactive oxidant. Also, support for the importance of the deprotonation was obtained by the reaction of **2** and **3** with *tert*-butyl peroxide or benzoyl peroxide. The (*tert*-butyl)OOH will react with **2** or **3** in the presence of water to give **5** but is unreactive with **1** or **13** unless base is added. Benzoyl peroxide contains no acidic protons yet is still an excellent oxidant as demonstrated by its routine use as a radical initiator. As predicted, this molecule does not react in any way with **2** or **3** or basic solutions of **1** or **13**.

Electrochemistry of Complexes. Another important consideration for the evaluation of reactivity involving formal oxidation state changes is the electrochemical potential of the reactants. Cyclic voltammograms of $[Mn^{III}(SALPN)(CH_3OH)]ClO_4$, **1**, Mn^{III}(SALPN)(AcAc), **2**, and $[Mn^{III}(SALPN)(CH_3O)]_2$, **3**, and $Mn^{III}_2(SALPN)_3$, **4**, are shown as Figure 6, and electrochemical parameters are reported in Table V. The monomeric **1** shows an irreversible one-electron reduction [Mn(III) → Mn(II), confirmed by rotating platinum electrode voltammetry][30] in acetonitrile at −106 mV vs SCE. We have observed no oxidative electrochemistry for this compound out to potentials of +1 V. In

(30) Rotating platinum electrode (RPE) voltammetry samples the properties of the bulk solution since the product of the electrode reaction is continuously swept away. This allows one to establish whether an oxidative or reductive current is passed. In contrast, cyclic voltammetry samples the electroactive species at the electrode surface and does not distinguish a priori whether the original state of the electroactive component was oxidized or reduced. For more details, see: *Electrochemical Methods: Fundamentals and Applications*; Bard, A. J.; Faulkner, L. R., John Wiley & Sons: New York, 1980.

contrast, **2**, **3**, and **4** show a quasi-reversible, one-electron oxidation around +550 mV. Irreversible one-electron reductions around −650 mV in acetonitrile (not shown) are also present. The dramatic stabilization of the Mn(IV) oxidation level is likely a result of two factors. Each complex contains one additional basic oxyanion per manganese which provides another negative charge to the Mn ion. In addition, **2**, **3**, and **4** each has a cis-β tetradentate SALPN coordinated, and there probably is a shift in potential associated with the change in donor placement and geometry about the Mn. Such an effect has been noted by Collins et al.[35] where distortion of tetradentate amide ligands resulted in an increase in the donor capacity of the amide nitrogens which, as a consequence, dramatically stabilized higher oxidation states. However, this effect is expected to be less pronounced in the MnSALPN case since the three-carbon backbone of the ligand is able to easily accommodate the cis-β configuration. Therefore, we expect the presence of an additional basic oxyanion to be the dominant factor in the stabilization of Mn(IV) in **2**, **3**, and **4** vs **1**.

It should be recognized that these potentials correspond to the formation of mononuclear Mn(IV) complexes. Indeed quantitative formation of $[Mn^{IV}(SALPN)(AcAc)]ClO_4$, **6**, can be achieved by bulk electrolysis at +700 mV. Dimers **3** and **4** also show one-electron oxidative waves at ~ +500 mV (Figure 6), and we have isolated mononuclear Mn(IV) complexes here via bulk electrolysis.[31] Note that only **5** is generated from **2**, **3**, and **4** in the presence of hydrogen peroxide, and the mononuclear Mn(IV) species generated by electrolysis do not react with H_2O_2 to give **5**. This suggests that the formation of **5** from H_2O_2 reaction with **2**, **3**, and **4** does not involve initial outer-sphere one-electron transfer to form such species as productive intermediates.

Isotopic Labeling Studies. Many of the synthetic procedures for reported bis-μ-oxo–manganese dimers involve the use of peroxidic oxidants in the presence of molecular oxygen as well as water.[38-41] Isotopically labeled water has been utilized to demonstrate exchange lability of bridging oxides in some systems.[39] However, the source of the original bridges when peroxidic oxidants are employed has not been previously demonstrated. We have investigated the bridging oxide source in this system by using ^{18}O-labeled H_2O_2 and water. The observation of a molecular ion in the negative ion FAB mass spectrum of **5** allowed for detection and quantitation of the labeled product.

Figure 7B shows the FAB mass spectrum of **5** formed by dropwise addition of ~0.1 M $H_2{}^{18}O_2$ in $H_2{}^{16}O$ to an acetonitrile solution of **2**. The observation of doubly labeled **5** (mass peak 706) demonstrates the direct incorporation of both peroxide oxygens. Also, no rise is observed above the statistical distribution of the mass peak at 704 (expected for the mixed-labeled product $\{[Mn^{IV}SALPN]_2(^{16}O,^{18}O)\}$) in spite of an ~550-fold molar excess of $H_2{}^{16}O$. This clearly demonstrates that the primary reaction mechanism excludes oxygen contained in water from entering the bridges in **5**.

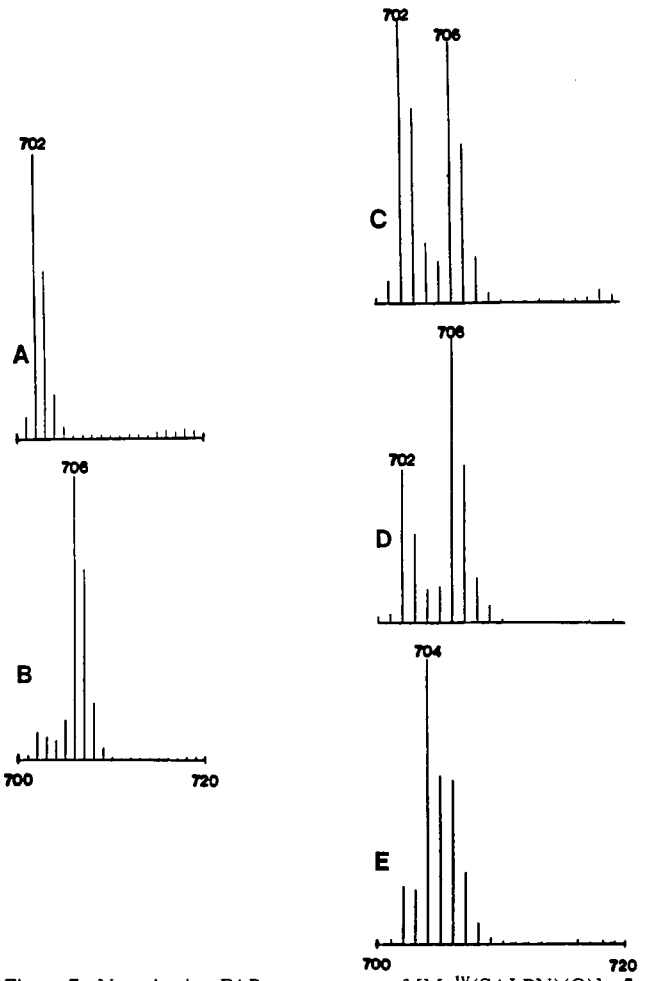

Figure 7. Negative ion FAB mass spectra of $[Mn^{IV}(SALPN)(O)]_2$, **5**, formed by reaction in acetonitrile of (A) $[Mn^{III}(SALPN)(AcAc)]$, **2**, plus $H_2{}^{16}O_2$, (B) **2** plus 0.1 M $H_2{}^{18}O_2$ in $H_2{}^{16}O$, (C) **2** plus a 50:50 mixture of $H_2{}^{18}O_2/H_2{}^{16}O_2$ in $H_2{}^{16}O$, and (D) $[Mn^{III}(SALPN)(OCH_3)]_2$ plus a 70:30 mixture of $H_2{}^{18}O_2/H_2{}^{16}O_2$ in $H_2{}^{16}O$, (E) **2** plus *tert*-butyl $^{16}O_2H$ and $H_2{}^{18}O$ (3-nitrobenzyl alcohol matrix). Parent ion peaks are $[Mn^{IV}(SALPN))^{16}O]_2$ = 702, $[Mn_2{}^{IV}(SALPN)_2{}^{18}O^{16}O]$ = 704, and $[Mn^{IV}(SALPN)^{18}O]_2$ = 706.

One can also address the question as to whether the operative mechanism allows for mixing of the incipient bridging oxides at this point or at any point after peroxide O–O bond cleavage. The mass spectra of **5** obtained by reaction of 50:50 and 40:60 mixtures of ~0.1 M aqueous $(H_2{}^{16}O)H_2{}^{16}O_2$ and $H_2{}^{18}O_2$ with **2** and **3** are shown in Figure 7, parts C and D, respectively. In both cases, the primary mass peaks are observed at 702 ($[Mn^{IV}(SALPN)(^{16}O)]_2$) and 706 ($[Mn^{IV}(SALPN)(^{18}O)]_2$). There is, again, no observed increase in the mixed dimer $\{[Mn^{IV}(SALPN)]_2(^{16}O,^{18}O)\}$ mass peak at 704. From these results we conclude that hydrogen peroxide is the source of the oxide oxygens in **5** and that *both atoms of oxygen originate from the same peroxide molecule*. Furthermore, this isotopic distribution could not be obtained through monomeric intermediates such as $LMn^{IV}O$ or $LMn^{V}O$ which further react to give **5**.

In contrast, the use of alkyl peroxides as oxidants yields very different results. Reaction of **2** or **3** with unlabeled (*tert*-butyl)OOH in the presence of $H_2{}^{18}O$ yields **5** containing an extensive amount of label. In this case, a mixture of $[Mn^{IV}(SALPN)(^{16}O)]_2$, $[Mn^{IV}(SALPN)(^{18}O)]_2$, and predominantly the mixed-labeled product $\{[Mn^{IV}(SALPN)]_2(^{16}O,^{18}O)\}$ is detected (Figure 7E).

Pathway of Formation of $[Mn^{IV}(SALPN)(O)]_2$, 5. If hydrogen peroxide is added to **2** or **3** in degassed acetonitrile, an instantaneous reaction occurs to give **5** in 100% yield. A mechanisitic

(31) The monomeric Mn(IV) formulation is supported by X-ray crystallography, elemental analysis, electrochemistry, magnetic moment, and EPR spectroscopy.

(32) Although it is physically unmeaningful to distinguish the oxidation potentials of two redox noninnocent centers within a single compound, in this case metal and peroxide, it can be conceptually useful in understanding the chemical process to view the system if one potential were fixed (metal) and the other (peroxide) is modified by each perturbation.

(33) Stomberg, R.; Olson, S.; Svenson, I.-B. *Acta Chem. Scand.* **1984**, *A38*, 653. Szentivanyi, H.; Stomberg, R. *Acta Chem. Scand.* **1983**, *A37*, 553. Stomberg, R.; Olson, S. *Acta Chem. Scand.* **1984**, *A38*, 801. Djordjevic, C.; Lee, M.; Sinn, E. *Inorg. Chem.* **1989**, *28*, 719.

(34) Ghosh, P.; Tyelklar, Z.; Karlin, K. D.; Jacobsen, R. R.; Zubieta, J. *J. Am. Chem. Soc.* **1987**, *109*, 6889.

(35) Expected statistical ratios between species could not be compared due to matrix effects inherent in FAB experiment. This assumption was confirmed in our samples by using known mixtures of **5** and $[Mn^{IV}O$-3,5-diClSALPN$]_2$.

(36) Anson, F. C.; Collins, T. J.; Gipson, S. L.; Keech, J. T.; Krafft, T. E.; Peake, G. T. *J. Am. Chem. Soc.* **1986**, *108*, 6593. Collins, T. J.; Keech, J. T. *J. Am. Chem. Soc.* **1988**, *110*, 1162.

(37) Collins, T. J. *J. Am. Chem. Soc.* **1988**, *11*, 4511. (b) Collins, T. J.; Powell, R. D.; Slebodnick, C.; Uffelman, E. S. *J. Am. Chem. Soc.* **1989**, *112*, 899.

(38) Nyholm, R. S.; Turco, A. *Chem. Ind.* (*London*) **1960**, 74.

(39) Cooper, S. R.; Calvin, M. *J. Am. Chem. Soc.* **1977**, *99*, 6623.

(40) Cooper, S. R.; Dismukes, G. C.; Klein, M. P.; Calvin, M. *J. Am. Chem. Soc.* **1978**, *100*, 7248.

(41) Plaskin, P. M.; Stoufer, R. C.; Mathew, M.; Palenik, G. J. *J. Am. Chem. Soc.* **1972**, *94*, 2121.

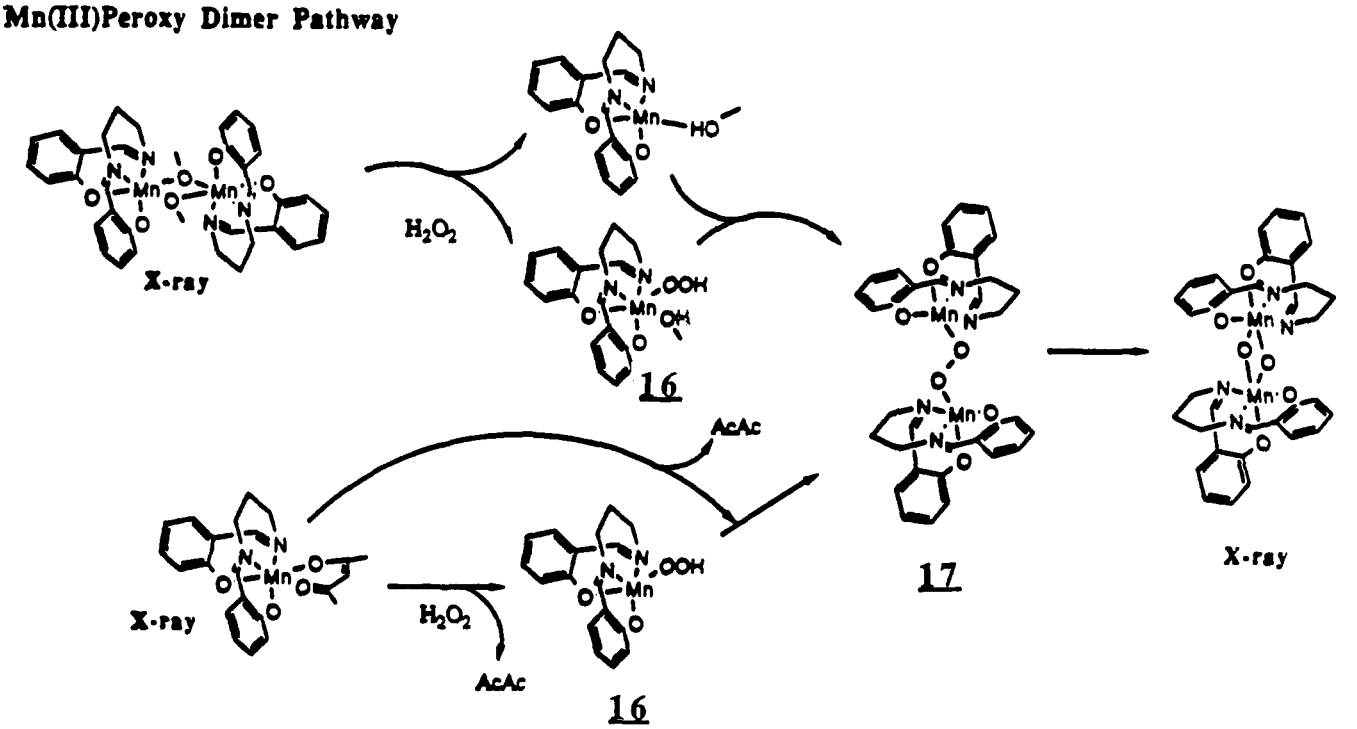

Figure 8. Proposed mechanism for the formation of $[Mn^{IV}(SALPN)(O)]_2$ through a Mn^{III}peroxy dimer pathway.

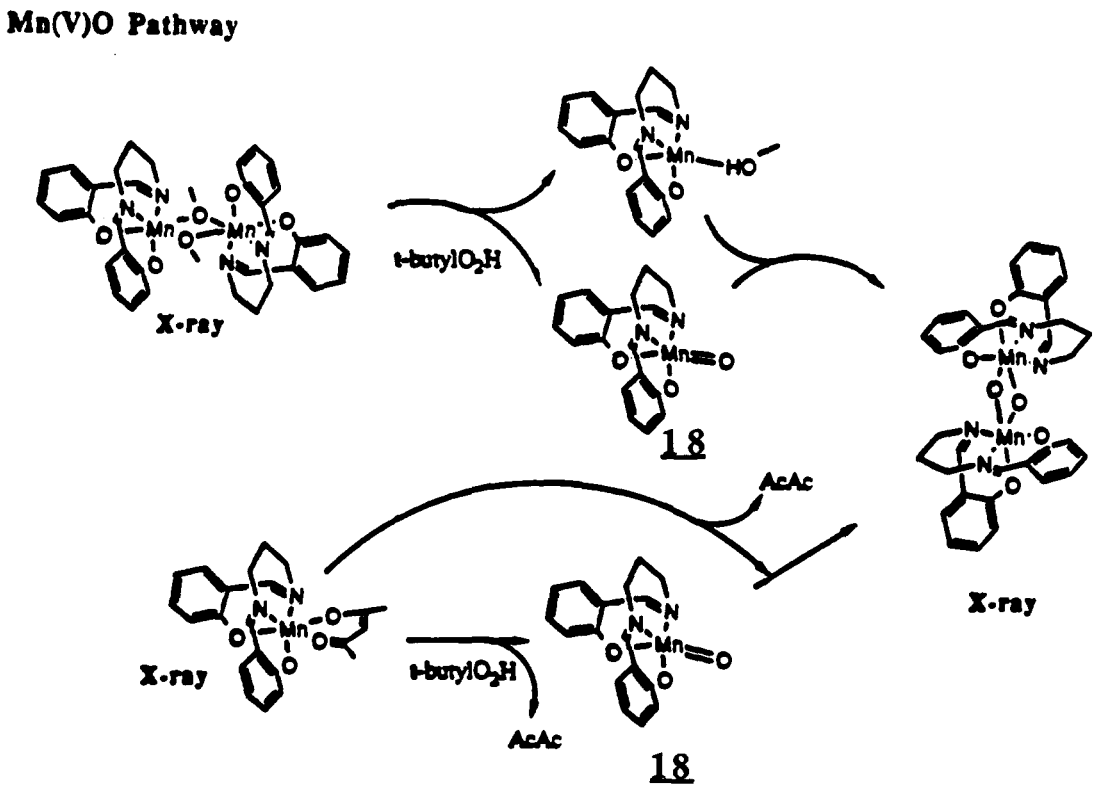

Figure 9. Proposed mechanism for the formation of $[Mn^{IV}(SALPN)(O)]_2$ through a $Mn^{V}O$ pathway.

pathway for the production of **5** by reaction of H_2O_2 with **2** and **3** is shown in Figure 8. This scheme is consistent with both the reactivity and isotopic labeling studies presented. It features H_2O_2 reacting via two successive deprotonation steps which utilize basic oxyanions associated with the Mn(III) precursors. The presence of some form of base is an absolute requirement as illustrated by the differential reactivity of **1** and **15** vs **2**, **3**, and **4**. Also, the ^1H NMR and electrochemical studies using triethylamine indicate that the abilities of oxyanions to stabilize the Mn(IV) oxidation level or to promote formation of cis-β "pretemplated" complexes are not the necessary characteristics which impart reactivity. We conclude that it is the proton-accepting feature of these anions which allows oxidation at the metal center and that deprotonation must, therefore, occur before cleavage of the peroxide bond. Thus, although H_2O_2 may transiently coordinate to **1** or **15** in solution, metal-centered oxidation does not occur prior to deprotonation. It is notable that association of the hydroperoxide anion to Mn(III) creates a ligand environment similar to that seen in **2** and **3**. Thus, deprotonation leads to stabilization of the Mn(IV) oxidation level at the metal center, and replacement of LM^{3+} for H^+ on H_2O_2 may make the coordinated peroxide molecule more easily reduced. Both of these factors should lead to an increase in the driving force

for internal oxidation of an intermediate such as **17** to yield **5**. A pathway as shown in Figure 8 is consistent with these observations.

We have no direct spectral evidence for the monomeric hydroperoxide intermediate **16** nor the peroxy-bridged dimer **17**. However, previous precedent from cuprous peroxide chemistry including the recent X-ray crystal structure[34] of $LCu^{I}OOCu^{I}L$ provides a structural analogy to the proposed **17**. It is obvious that a monomeric intermediate must be involved at some point in the reaction of H_2O_2 with **2** since the starting material is monomeric. Such a statement is less intuitive with **3** which is dimeric in solution as indicated by ^1H NMR. To confirm the existence of a monomeric intermediate, a 50:50 mixture of **3** and $[Mn^{III}(3,5\text{-diCl-SALPN})(OCH_3)]_2$, **12**, was allowed to react with H_2O_2 in acetonitrile. The same reaction using **2** and $Mn^{III}(3,5\text{-diCl-SALPN})(AcAc)]$, **10**, was run as a control. In each case, a mixture of **5**, $Mn^{IV}_2(3,5\text{-diCl-SALPN})(SALPN)(O)_2$, and $[Mn^{IV}(3,5\text{-diCl-SALPN})(O)]_2$ was obtained.[35] When mixed, **5** and $[Mn^{IV}(3,5\text{-diCl-SALPN})(O)]_2$ will not scramble on the time scale of the experiment to give $Mn^{III}_2(3,5\text{-diCl-SALPN})(SALPN)(OCH_3)_2$ or $Mn^{IV}_2(3,5\text{-diCl-SALPN})(SALPN)(O)_2$, respectively. Due to the exchange lability of Mn(III) one might expect **3** and **12** to scramble more rapidly. However, electrochemical analysis of a mixture of **3** and **12** in acetonitrile indicates no mixing on the time scale of this experiment. Therefore, insertion of hydrogen peroxide into **3** requires the dissociation of the dimer prior to cleavage of the peroxide bond. Furthermore, these observations argue for dissociation which is instigated by H_2O_2 rather than a predissociation step. We prefer the formulation of **16** converting to **17** as the intermediates in this process; however, on the basis of these data, we cannot exclude a Stomberg type peroxo monomer[33] (e.g., $[(SALPN)Mn^{III}(O_2)]^-$) as seen for V(V) complexes which could then react with a monomeric $Mn(SALPN)^+$ to form **5**. Interpretation of the peroxide oxidation of **2** is straightforward, following closely the pathway proposed for **3**.

The formation of **5** from **2** and **3** and **4** using *tert*-butyl hydroperoxide as the oxidant appears to follow a pathway very different from that of reaction with H_2O_2. The reaction is not instantaneous, requiring a number of hours (at room temperature) and the presence of water. *tert*-Butyl hydroperoxide lacks a second dissociable proton. To proceed to form **5** it could lose *tert*-butyl cation which would lead to conservation of both *unlabeled* peroxide oxygens in **5**. However, the operative mechanism allows extensive mixing of labeled water. The isotopic pattern is consistent with the initial formation of $Mn^{V}O(SALPN)$, **18**, which then reacts with an equivalent of $Mn^{III}SALPN(OH)$ to give **5**. Although numerous pathways could be envisioned which might fit these data, this scheme is most attractive in light of known chemistry. $Mn^{V}OL$ complexes have now been structurally characterized[37] which utilize similar ligands containing amido rather than imino linkages. These have been shown to exchange labeled water into the manganyl-oxo.[37b] Thus, in the pathway shown in Figure 9, the label is expected to scramble through exchange in both the Mn(III) and Mn(V) intermediates. The generation of an $Mn^{V}O(SALEN)$ (also shown to exchange labeled water into the manganyl-oxo) by reaction of an Mn(III) precursor with (*tert*-butyl)OOH has been reported by Kochi.[22] Epoxidation of olefins was observed in these studies and attributed to a Mn(V) species. We have also observed epoxidation of cyclohexene under conditions which form **5** in our system. In Kochi's system, the SALEN complex can form an Mn(IV) dimer of proposed structure $LMn^{IV}OMn^{IV}L$ via coupling of an $Mn^{V}O$ with an Mn(III). However, a dioxo dimer similar to **5** is not isolated because the SALEN ligand cannot adopt the cis-β binding mode.

Finally, the reaction of **4** with dioxygen apparently follows a different (or at least additional) pathway since direct oxidation by $^{16}O_2$ in the presence of a small amount of $^{18}OH^-$ leads to scrambling of the label in the oxo bridges. This is in contrast to the hydrogen peroxide oxidations for which labeling of the bridging oxides was not dependent on the presence of either $H_2{}^{18}O$ or $^{18}OH^-$. We are presently investigating the differences between dioxygen and hydrogen peroxide oxidations and will report this work separately.

In summary, the products and reaction pathways for the oxidation of Mn(III) Schiff base complexes with peroxides are dependent both on the ligand and the oxidant. The $[Mn^{IV}SALPN(O)]_2$ can be prepared either through an $LMn^{III}(O\text{-}O)Mn^{III}L$ dimer or by coupling of $Mn^{V}O$ and $Mn^{III}(OH)$ depending on the availability of dissociable protons on the oxidant. In contrast, a monooxo-bridged Mn(IV) dimer has been implicated in the oxidation of $Mn^{III}SALEN$ precursors.[22] In this case, coupling of $Mn^{V}O$ and $Mn^{III}(OH)$ was the exclusive mechanism, and the dioxo dimer could not be formed, presumably because the steric demands of the SALEN ligand are too great.

Acknowledgment. The authors thank Dr. Joseph A. Bonadies and Dr. Myoung Soo Lah for many useful discussions and assistance in many experimental studies. The FAB mass spectra were recorded by Mr. James Windak, and elemental analyses were completed by Mr. William Hatton. Discussions with Professor James Penner-Hahn on the chemistry of the Mn catalase and Professor Robert Kuczkowski on isotope labeling studies were of particular benefit to this project. This work was supported by NIH (GM 39406) and an Alfred P. Sloan Fellowship to V. L. Pecoraro and a Dow Britton Predoctoral Fellowship to Erlund J. Larson.

Supplementary Material Available: Tables VI–IX of fractional atomic coordinates for all atoms, Tables X–XIII of anisotropic thermal parameters, Tables XIV–XVII of the complete set of bond distances, Tables XVIII–XXI of the complete set of bond angles, and Table XXVI of crystallographic parameters and Figures 10, 11, 12, and 13 of complete numbering schemes for **7**, **2**, **12**, and **4**, respectively (38 pages); Tables XXII–XXV of observed and calculated structure factors for **7**, **2**, **12**, and **4**, respectively (58 pages). Ordering information is given on any current masthead page.